International Journal of Solids and Structures 47 (2010) 1764–1774

Contents lists available at ScienceDirect

International Journal of Solids and Structures

journal homepage: www.elsevier.com/locate/ijsolstr

Multiscale structural design of columns made of regular octet-truss lattice material

Mostafa S.A. Elsayed, Damiano Pasini *

Department of Mechanical Engineering, McGill University, Montreal, QC, Canada H3A 2K6

ARTICLE INFO

Article history:
Received 2 November 2009
Received in revised form 22 January 2010
Available online 7 March 2010

Keywords:
Lattice material
Stretching dominated
Octet-truss
Multiscale structural design

ABSTRACT

This paper focuses on the structural design of the microscopic architecture of a lattice material with regular octet-truss cell topology and on the multiscale design of an axially loaded member manufactured of this type of cellular solid. The rationale followed here hinges on the coincidence of the failure modes of a stretching dominated lattice material, which experiences two types of microscopic failure modes, namely, elastic buckling and plastic yielding. A lattice material that fails by the elastic buckling of its cell elements without reaching the plastic yielding is far from optimum. To avoid this event and improve the material strength, we first start to tailor the structural efficiencies of the cell elements. We show that by shaping the cell element cross-sections, the lattice material buckling resistance can increase until it equals the cell element yield strength, thereby exploiting fully the lattice material strength. The coincidence of these two failure modes is the structural criterion used to develop selection charts for the microstructural design of the octet-truss lattice material. In the second part of the paper, we examine the design of a structural column manufactured by regular octet-truss lattice material. We show that to maximize the structural failure resistance at both the structural and the material levels, the global buckling and the yielding failure of the column must occur simultaneously with the microscopic failure modes of the lattice material, namely the local buckling and the yielding of its microscopic cell elements. The paper concludes by illustrating how the micro-truss geometry and the column cross-section can be simultaneously designed to fully exploit the strength of the material and the overall macrostructure.

1. Introduction

A lattice material is a micro-structured material whose building blocks are the material cells. It is generally classified into Stretching Dominated Lattice Materials (SDLM) and Bending Dominated Lattice Materials (BDLM) (Ashby, 2005). Microscopic structural analysis of the SDLM shows that its stiffness and strength scale up with the densities ratio of the cellular material to the solid material, $\bar{\rho}_L$, while the stiffness and strength of the BDLM are governed, respectively, by $\bar{\rho}_L^2$ and $\bar{\rho}_L^{3/2}$ (Deshpande et al., 2001; Deshpande and Fleck, 2001). The different scaling laws have a strong impact on the strength and stiffness of the material. For example, at $\bar{\rho} = 0.01$, the SDLM is 100 times stiffer and 10 times stronger than the BDLM.

The cell elements of a SDLM are essentially loaded in axial tension or compression. An idealized representation of the SDLM is a microscopic truss structure with pin-joints that allow rotations. However, in practice these nodes are manufactured as rigid. As a result, secondary bending stresses develop in the cell elements but at a level almost negligible compared to that generated by the axial stresses, which ultimately govern the SDLM failure. These modes of failure include the plastic yielding in tension and the elastic buckling and plastic yielding in compression. Characterization of the SDLM shows that low density lattice materials always fail by elastic bucking even when the macroscopic load is tension (Deshpande et al., 2001). A lattice material that fails by elastic buckling is far from optimum, since the element becomes unstable without fulfilling its potential yield resistance, where the element fails in the elastic region at a loading lower than the load inducing its plasticity. To improve this behavior, researchers found critical values of the relative densities for different cell topologies at which the buckling failure of the cell elements can be avoided (Fan et al., 2008). Such strength improvement was achieved at the expense of the lattice material density, which therefore had to be increased, as the cell element's slenderness ratio was decreased by either lowering its length or by scaling up its radius of gyration. However, no attention to the potential of shaping the cross-section was considered. So far, studies on lattice material have considered microscopic cell elements with circular solid cross-sections. A few studies have investigated experimentally, the behavior of lattice material with cylindrical hollow cross-sections (Wadley, 2002). Due to recent development in micro-manufacturing technologies, namely rapid prototyping and rapid manufacturing (Kruth et al., 2005; Rochus

* Corresponding author. Address: Macdonald Engineering Building, Room 372, 817 Sherbrooke St West, Montreal, QC, Canada H3A 2K6. Tel./fax: +1 514 398 6295.
E-mail addresses: mostafa.elsayed@mail.mcgill.ca (M.S.A. Elsayed), damiano.pasini@mcgill.ca (D. Pasini).

0020-7683/$ - see front matter Crown Copyright © 2010 Published by Elsevier Ltd. All rights reserved.
doi:10.1016/j.ijsolstr.2010.03.003

et al., 2007; Waterman and Dickens, 1994), shaping microscopic structural elements in more efficient geometries has become feasible. Such progress on the manufacturing process encourages exploiting the potential of shaping and sizing the cross-sections of the cell elements to increase the lattice material strength.

This paper examines the impact of shaping the cell element cross-sections of the lattice material on its structural performance. We resort to recent studies that have investigated the effect of cross-section geometry on the performance of macroscale structures under different loading (Pasini, 2007; Pasini et al., 2003, 2006). We first illustrate that enhancing the cell elements' buckling resistance by shaping their cross-sections allows the design of low density lattice material that fail by plastic yielding rather than buckling and, thus, fully exploit the material strength. Then, we examine an axially loaded member manufactured of octet-truss lattice material with the aim of fully exploiting its load carrying capacity. For this purpose, the structural member is optimized by imposing the coincidence between three failure modes, namely, the local buckling (buckling of the microscopic cell elements), global buckling (buckling of the macroscopic structure) and the plastic yielding of the lattice material. Design charts are developed to enable a multiscale design of a macroscale member subjected to axial compression and manufactured of regular octet-truss lattice material. The charts help compare and select simultaneously the micro- and the macrostructural design.

2. Description of the regular octet-truss cell

This work focuses on a lattice material with regular octet-truss cell topology. Fig. 1 shows the microscopic topology of a unit cell of the lattice material examined here. The unit cell can be viewed as a regular octahedron core that is surrounded by eight regular tetrahedrons distributed on its eight faces. The cell has a Face Centered Cube (FCC) lattice structure with cubic symmetry generating a material with an isotropic behavior (Renton, 2002); its nodes are similarly situated with 12 cell elements connectivity at each node.

Determinacy analysis of the pin-jointed version of this microscopic topology shows that this unit cell is statically and kinematically determinate. However, when the unit cell is tessellated to generate the periodic material, the resulting microstructure becomes highly redundant and statically indeterminate, a feature common to all stretching dominated cell topologies (Guest and Hutchinson, 2003).

In the literature, works on the octet-truss lattice material consider the geometry of each cell element as uniform along their length and with circular solid cross-section. It has been demonstrated that a lattice material that fully exploits the yield strength of the cell elements can be designed at the expenses of its relative density (Fan et al., 2008). As a result, the lattice material density must be increased to critical values, under which the cell elements buckle. In this work, we circumvent this strategy. Rather than increasing the material density, we chose to strengthen the buckling resistance of each cell element by shaping its cross-sections into a more efficient geometry.

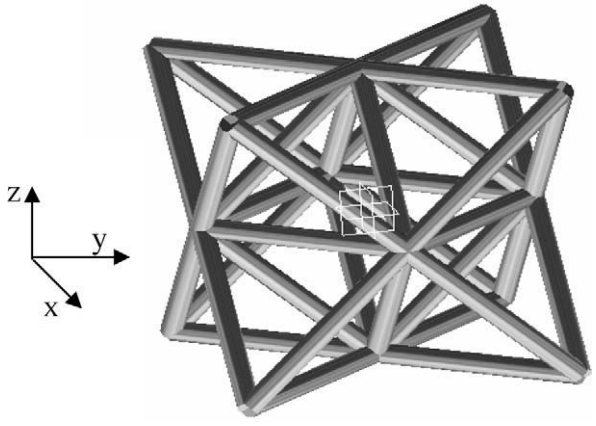

Fig. 1. Structure of a unit cell of the regular octet-truss lattice material.

3. Geometric variables

To model the effective properties of the regular octet-truss lattice material, we define a range of modeling parameters. Fig. 2 shows the geometrical details of a macroscopic mechanical member that is hierarchically parameterized and manufactured of a lattice material. On the microscale, three parameters S, D and D_0 are defined for a cell element cross-section of an arbitrary shape and size, where S, D and D_0 are, respectively, the shape, the envelope, and the envelope of a reference square. To model the efficiency of a cross-section, dimensionless parameters, named as shape transformers, can be defined to classify shapes into families and classes as well as to describe their geometrical properties (Pasini, 2007).

For example, the shape transformers of the area and of the second moment of area of a cross-section are defined as:

$$\psi_A = \frac{A}{A_D} \tag{1a}$$

$$\psi_I = \frac{I}{I_D} \tag{1b}$$

where ψ_A and ψ_I are, respectively, the area and the second moment of area shape transformers; A and I are, respectively, the area and the second moment of area of an arbitrary cross-section and A_D and I_D are the area and the second moment of area of the cross-section envelope, respectively.

Shape transformers can be used to define the cross-section efficiencies of alternative shapes for given loading requirements. For example, the cross-section geometric efficiency, λ, controlling the bending stiffness and the elastic buckling can be defined as:

$$\lambda = \frac{\psi_I}{\psi_A} \tag{2}$$

On the other hand, the effect of scaling the cross-section size is governed by two dimensionless multipliers, u and v, where u and v scale, respectively, the width B_0 and the height H_0 of the reference square envelope, D_o, to the required dimensions of the cross-section. As a result, u and v can be expressed as:

$$u = \frac{B}{B_0} \tag{3a}$$

$$v = \frac{H}{H_0} \tag{3b}$$

where B and H are, respectively, the width and the height of the cross-section envelope. Using Eqs. (1) and (3), the area and the second moment of area of a cross-section can be expressed as:

$$A = \psi_A u v A_0 \tag{4a}$$

$$I = \psi_I u v^3 I_0 \tag{4b}$$

where A_0 and I_0 are, respectively, the area and the second moment of area of the reference square. For the shape of the cross-section, shown in Fig. 2, the shape transformers of the second moment of area and that of the area, ψ_I and ψ_A, can be expressed as:

$$\psi_I = 1 - cd^3 \tag{5a}$$

$$\psi_A = 1 - cd \tag{5b}$$

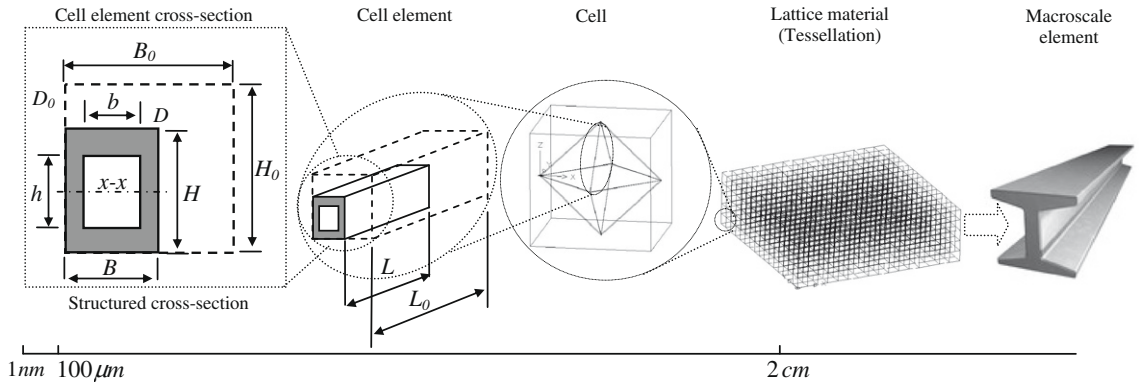

Fig. 2. Multiscale geometrical details of macroscopic member manufactured of lattice material.

where $c = b/B$ and $d = h/H$ and $0 \leqslant c \leqslant 1$ and $0 \leqslant d \leqslant 1$. By using Eq. (5), the cross-section efficiency is expressed as:

$$\lambda = \frac{1 - cd^3}{1 - cd} \tag{6}$$

A change of c and d in the interval of $[0,1]$ results in values of ψ_I and ψ_A in the range of $[0,1]$ while λ range is $[1,3]$. Similar formulation can be expressed for different shape classes, e.g. ellipses and diamonds (Pasini, 2007; Pasini et al., 2003, 2006).

The limiting curves that show the variation of ψ_I and ψ_A with the variation of the two parameters c and d is plotted in Fig. 3 for the three cross-section shapes considered in this study.

In Fig. 3, the bending efficiency necessary to assess the bending and the buckling resistance of a cross-section can be evaluated by computing the tangent of the angle formed by the line extending from the origin of the graph to the point representing the shape of each cross-section.

The buckling resistance of the microscopic cell element of the lattice material is governed by the radius of gyration, r_g, of the element cross-section, besides by its length. The radius of gyration is linked to the second moment of area by the expression:

$$I = Ar_g^2 \tag{7}$$

To express Eq. (7) in terms of the shape transformers, we substitute Eqs. (4) and (5) into Eq. (7) and use Eq. (2) to obtain the following expression (Pasini et al., 2003):

$$r_g^2 = \lambda v^2 r_{g0}^2 \tag{8}$$

where r_{g0} is the radius of gyration of the reference cross-section.

In addition to modeling the cross-section geometry, we introduce also another parameter, s, which models the length L of the cell element with respect to the length L_0 of a reference prismatic element. Similar to u and v, this scaling multiplier is expressed as:

$$s = \frac{L}{L_0} \tag{9}$$

Expressions (1)–(9) are used in this work to model the geometrical properties at the micro- and macroscopic scales of the structure. To distinguish between scale parameters, we use throughout the whole paper the subscript "e" for the microscopic parameters and "G" for the macroscopic ones.

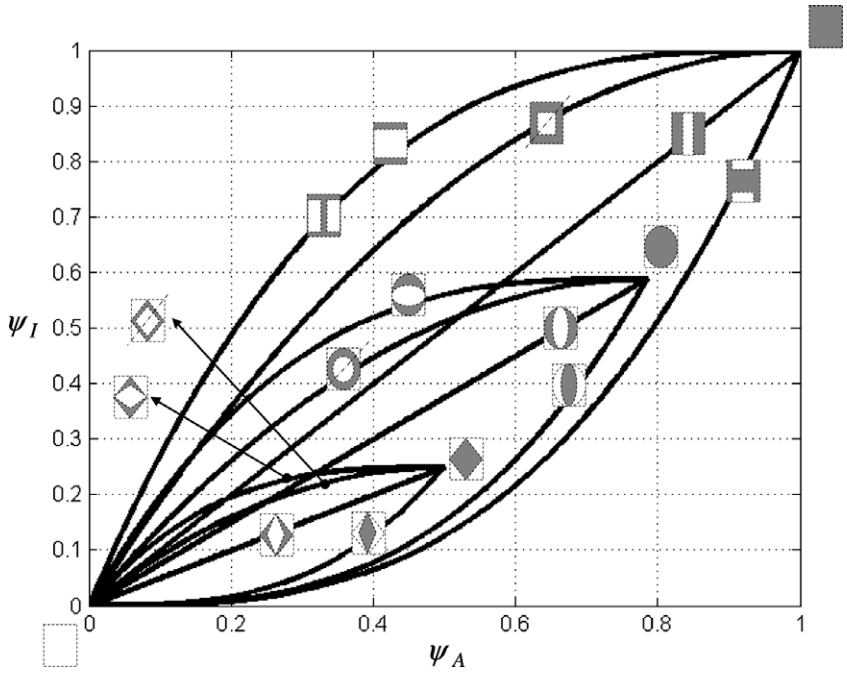

Fig. 3. Variation of the shape transformers of the cross-section area and second moment of area for different cross-section shapes.

4. Modeling the effective properties of the octet-truss lattice material

In this section, the effective properties of the regular octet-truss lattice material are formulated as a function of the shape properties of the cell element cross-sections. Cross-sections with double symmetry with respect to their principal axes are examined. The properties considered include the material density, the elastic and the strength properties and the material collapse surfaces. For comparison, we report here also the formulations of the regular octet-truss lattice material found in the literature (Deshpande et al., 2001), where the cell element geometry of the lattice material is assumed to be uniform with circular solid cross-section. The properties of previous models are identified here with the suffix "*a*"; whereas the suffix "*b*" is used for our models, which are governed by the parameters presented in Section 3. It is assumed that the solid material used in manufacturing the lattice material is elastic-perfectly plastic and has an isotropic behavior with a Poisson's ratio of $\upsilon_0 = 1/3$.

4.1. Relative density

If we assume that the mass of the boundary elements of the unit cell are divided equally among the neighboring cells, then the relative density of the regular octet-truss lattice material can be expressed as:

$$\bar{\rho}_{La} = \frac{\rho_{La}}{\rho_0} = \left(6\pi\sqrt{2}\right)\left(\frac{a_e}{L_e}\right)^2 \tag{10a}$$

$$\bar{\rho}_{Lb} = \frac{\rho_{Lb}}{\rho_0} = \left(6\sqrt{2}\right)\left(\frac{A_{e0}}{L_{e0}^2}\right)\left(\frac{\psi_{eA} u_e \upsilon_e}{s_e^2}\right) \tag{10b}$$

where a_e is the radius of the cell element cross-section. $\bar{\rho}_L$ is the relative density of the lattice material, ρ_L is the density of the lattice material and ρ_0 is the density of the solid material used to manufacture the lattice material.

4.2. Elastic properties

The regular octet-truss cell geometry has a cubic symmetry, which generates a material with isotropic properties (Renton, 2002). The compliance matrix of an isotropic material can be expressed as:

$$[C] = \frac{1}{E_L}\begin{bmatrix} 1 & -\upsilon_L & -\upsilon_L & 0 & 0 & 0 \\ -\upsilon_L & 1 & -\upsilon_L & 0 & 0 & 0 \\ -\upsilon_L & -\upsilon_L & 1 & 0 & 0 & 0 \\ 0 & 0 & 0 & 2(1+\upsilon_L) & 0 & 0 \\ 0 & 0 & 0 & 0 & 2(1+\upsilon_L) & 0 \\ 0 & 0 & 0 & 0 & 0 & 2(1+\upsilon_L) \end{bmatrix} \tag{11}$$

where υ_L and E_L are, respectively, the lattice material Poisson's ratio and Young's modulus.

By using the direct stiffness method, the relative Young's modulus of the octet-truss lattice material can be expressed as:

$$\bar{E}_{La} = \frac{E_{La}}{E_0} = \frac{2\pi\sqrt{2}}{3}\left(\frac{a_e}{L_e}\right)^2 \tag{12a}$$

$$\bar{E}_{Lb} = \frac{E_{Lb}}{E_0} = \frac{2\sqrt{2}}{3}\left(\frac{A_{e0}}{L_{e0}^2}\right)\left(\frac{\psi_{eA} u_e \upsilon_e}{s_e^2}\right) \tag{12b}$$

where E_L, $\bar{E}_L$ and E_0 are, respectively, the Young's modulus of the lattice material, the relative Young's modulus of the lattice material and the Young's modulus of the solid material.

Combining Eq. (12a) to Eq. (10a) and Eq. (12b) to Eq. (10b) results in:

$$\bar{E}_L = \frac{E_L}{E_0} = \frac{1}{9}\bar{\rho}_L \tag{13}$$

The Poisson's ratio of the regular octet-truss lattice material is found to be $\upsilon_L = 1/3$. Therefore, the full compliance matrix of the regular octet-truss lattice material can be formulated as:

$$[C] = \frac{1}{E_0\bar{\rho}_L}\begin{bmatrix} 9 & -3 & -3 & 0 & 0 & 0 \\ -3 & 9 & -3 & 0 & 0 & 0 \\ -3 & -3 & 9 & 0 & 0 & 0 \\ 0 & 0 & 0 & 24 & 0 & 0 \\ 0 & 0 & 0 & 0 & 24 & 0 \\ 0 & 0 & 0 & 0 & 0 & 24 \end{bmatrix} \tag{14}$$

The relative shear modulus, $\bar{G}_L$, and the relative bulk modulus, $\bar{\kappa}_L$, of the regular octet-truss lattice material can then be expressed as:

$$\bar{G}_L = \frac{G_L}{G_0} = \left(\frac{E_L}{2(1+\upsilon_L)}\right)\Big/ G_0 = \frac{\bar{\rho}_L}{9} \tag{15}$$

$$\bar{\kappa}_L = \frac{\kappa_L}{\kappa_0} = \left(\frac{E_L}{3(1-2\upsilon_L)}\right)\Big/ \kappa_0 = \frac{\bar{\rho}_L}{9} \tag{16}$$

where G_0 and κ_0 are, respectively, the shear and the bulk moduli of the solid material.

Eqs. (13), (15) and (16) show that the elastic properties of the regular octet-truss lattice material are independent of the geometrical attributes of the cell elements. It can be realized that the ratio of the relative elastic moduli to the relative density is "1/9", a constant that depends on the topology of the regular octet-truss cell.

4.3. Strength properties

4.3.1. Plastic yield strength

By using the direct stiffness method, axial and shear yield strengths of the regular octet-truss lattice material can be formulated as:

$$\bar{\sigma}_{yLa} = \frac{\sigma_{yLa}}{\sigma_{y0}} = \pi\sqrt{2}\left(\frac{a_e}{L_e}\right)^2 \tag{17a}$$

$$\bar{\tau}_{yLa} = \frac{\tau_{yLa}}{\tau_{y0}} = \frac{\pi}{\sqrt{2}}\left(\frac{a_e}{L_e}\right)^2 \tag{17b}$$

$$\bar{\sigma}_{yLb} = \frac{\sigma_{yLb}}{\sigma_{y0}} = \sqrt{2}\left(\frac{A_{e0}}{L_{e0}^2}\right)\left(\frac{\psi_{eA} u_e \upsilon_e}{s_e^2}\right) \tag{18a}$$

$$\bar{\tau}_{yLb} = \frac{\tau_{yLb}}{\tau_{y0}} = \sqrt{2}\left(\frac{A_{e0}}{L_{e0}^2}\right)\left(\frac{\psi_{eA} u_e \upsilon_e}{s_e^2}\right) \tag{18b}$$

where σ_{y0} and σ_{yL} are the direct yield strengths of the solid material and the lattice material, respectively. τ_{y0} and τ_{yL} are the shear yield strengths of the solid material and the lattice material, respectively.

Combining Eqs. (17a) and (18a) into Eq. (10a) as well as combining Eqs. (17b) and (18b) into Eq. (10b) give:

$$\bar{\sigma}_{yL} = \frac{1}{6}\bar{\rho}_L \tag{19a}$$

$$\bar{\tau}_{yL} = \frac{1}{6}\bar{\rho}_L \tag{19b}$$

where $\tau_{yL} = \frac{1}{2}\sigma_{yL}$ and $\tau_{y0} = \frac{1}{2}\sigma_{y0}$ are obtained from the Mohr's circle of an isotropic material in pure shear.

Eq. (19) shows that, also the yield strength properties of the regular octet-truss lattice material are independent of the cell elements geometry where the ratio of lattice material relative direct and shear strengths to its relative density is a constant.

4.3.2. Elastic buckling strength

The Euler critical buckling load of an axially loaded member in compression is expressed as:

$$P_{cr} = k^2 \frac{\pi^2 EI}{L^2} \tag{20}$$

where E is the Young's modulus of the material, I is the smallest second moment of area of the member cross-section, L is the length of the member and k is a factor that depends on the rotational stiffness of the member end boundaries. For a pin-jointed element where joint rotation is freely allowed, $k = 1$. If the rotation is fully constrained by fixed boundary conditions, then $k = 2$. In practice, the value of the factor k of a SDLM is between 1 and 2. We idealize the octet-truss lattice material as a pin-jointed micro-truss structure with $k = 1$, which is a safe design assumption.

Eqs. (8) and (9) along with Eq. (20) are used to express the critical buckling stress of the regular octet-truss lattice material as:

$$\bar{\sigma}_{ea}^{cr} = \frac{\sigma_{ea}^{cr}}{\sigma_{y0}} = \left(\frac{2\pi^3\sqrt{2}}{3}\right)\left(\frac{E_0}{\sigma_{y0}}\right)\left(\frac{a_e}{L_e}\right)^4 \tag{21a}$$

$$\bar{\sigma}_{eb}^{cr} = \frac{\sigma_{eb}^{cr}}{\sigma_{y0}} = \left(\pi^2\sqrt{2}\right)\left(\frac{r_{eg0}^2 A_{e0}}{L_{e0}^4}\right)\left(\frac{E_0}{\sigma_{y0}}\right)\left(\frac{\psi_{el} u_e v_e^3}{s_e^4}\right) \tag{21b}$$

where $\bar{\sigma}_e^{cr}$ and σ_e^{cr} are, respectively, the relative critical buckling strength and the critical buckling strength of the regular octet-truss lattice material.

By combining Eq. (21a) to (10a), and (21b) to (10b), Eq. (21) can be modified as:

$$\bar{\sigma}_{ea}^{cr} = \frac{\sigma_{ea}^{cr}}{\sigma_{y0}} = \left(\frac{\pi}{54\sqrt{2}}\right)\left(\frac{E_0}{\sigma_{y0}}\right)\bar{\rho}_L^2 \tag{22a}$$

$$\bar{\sigma}_{eb}^{cr} = \frac{\sigma_{eb}^{cr}}{\sigma_{y0}} = \left(\frac{\pi^2}{36\sqrt{2}}\right)\left(\frac{r_{eg0}^2}{A_{e0}}\right)\left(\frac{E_0}{\sigma_{y0}}\right)\left(\frac{\lambda_e}{\psi_{eA}}\right)\left(\frac{v_e}{u_e}\right)\bar{\rho}_L^2 \tag{22b}$$

From Eq. (22a), it can be seen that the critical buckling strength of the lattice material with uniform cell elements of a circular solid cross-section is a function of the material relative density as well as the solid material properties. On the other hand, Eq. (22b) shows that, in lattice materials with shaped cell element cross-sections, the critical buckling strength is also a function of the geometrical attributes of the cell element cross-section.

To avoid failure by buckling, we impose the condition:

$$\bar{\sigma}_e^{cr} \geqslant \bar{\sigma}_{yL} \tag{23}$$

Substituting Eqs. (17a) and (22a) into inequality (23) gives:

$$\bar{\rho}_{La} \geqslant \left(\frac{6\sqrt{2}}{\pi}\right)\left(\frac{\sigma_{y0}}{E_0}\right) \tag{24}$$

The equality form of expression (24) is the critical relative density, $\bar{\rho}_{La}^*$, of the regular octet-truss lattice material with circular solid cell element cross-sections. As formulated, $\bar{\rho}_{La}^*$ is only a function of the solid material properties. The geometrical attributes of the cell element are included together with the cell topology properties in the constant $\left(\frac{6\sqrt{2}}{\pi}\right)$.

To formulate the critical relative density, $\bar{\rho}_{Lb}^*$, as a function of the geometrical properties of the cell element cross-section, we combine Eqs. (18a) and (22b) with inequality (23), and write:

$$\bar{\rho}_{Lb}^* = \left(\frac{6\sqrt{2}}{\pi^2}\right)\left(\frac{A_{e0}}{r_{eg0}^2}\right)\left(\frac{\sigma_{y0}}{E_0}\right)\left(\frac{u_e}{v_e}\right)\left(\frac{\psi_{eA}}{\lambda_e}\right) \tag{25}$$

The contribution of the shape of the cell element cross-section can be isolated by rearranging Eq. (25) as:

$$\frac{\bar{\rho}_{Lb}^*}{\left(\frac{6\sqrt{2}}{\pi^2}\right)\left(\frac{A_{e0}}{r_{eg0}^2}\right)\left(\frac{\sigma_{y0}}{E_0}\right)\left(\frac{u_e}{v_e}\right)} = \left(\frac{\psi_{eA}}{\lambda_e}\right) \tag{26}$$

The effect of the cross-section efficiency and area shape transformer on the lattice material critical relative density is shown in Fig. 4, where Eq. (26) was plotted for the three shape families (rectangular, elliptical and diamond) considered in this work. For a given area shape transformer, ψ_{eA}, each family of cross-section shapes generates its own specific trend of critical relative density which provides the minimum critical density that minimizes Eq. (26). From Fig. 4, we gather that for the whole range of ψ_{eA} the family of the rectangles has the potential to minimize $\frac{\psi_{eA}}{\lambda_e}$ better than the other shapes.

4.4. Collapse surfaces

A lattice material subjected to static loading encounters four types of collapses, namely, plastic yielding (strength failure), elastic buckling (instability failure), creep (deformation increase under constant loading) and relaxation (load carrying capacity decrease under constant deformation). In the following analysis, strength and stability collapses are examined.

4.4.1. Yield collapse

The elements of a SDLM are always loaded axially, either in tension or compression. Unlike the collapse surfaces of solid materials (Beer and Johnston, 1981) which, in the case of ductile materials, can be derived by using a static failure criterion, such as the maximum shear stresses (Tresca) or the maximum distortion energy (von Mises), the yield collapse of a SDLM is governed by the axial yielding of the microscopic cell elements through a load transformation from the macroscopic stress field into the microscopic elements. If we assume that each microscopic element of the octet-truss lattice material has a slenderness ratio that prevents buckling, then all the cell members fail by plastic yielding. Following the approach of Deshpande et al. (2001), we consider a load case where the regular octet-truss cell is loaded by two forces in the x and the z principal directions, as shown in Fig. 1. If the yield strength, σ_{y0}, is the same in tension and compression, the elastic yielding collapse surface in the x–z-plane can be formulated as:

$$\left|\frac{\sigma_{xxa}}{\sigma_{y0}}\right| + \left|\frac{\sigma_{zza}}{\sigma_{y0}}\right| \leqslant 2\pi\sqrt{2}\left(\frac{a_e}{L_e}\right)^2 \tag{27a}$$

$$\left|\frac{\tau_{xza}}{\sigma_{y0}}\right| + \left|\frac{\sigma_{zza}}{2\sigma_{y0}}\right| \leqslant \pi\sqrt{2}\left(\frac{a_e}{L_e}\right)^2 \tag{27b}$$

$$\left|\frac{\sigma_{xxb}}{\sigma_{y0}}\right| + \left|\frac{\sigma_{zzb}}{\sigma_{y0}}\right| \leqslant 2\sqrt{2}\left(\frac{A_{e0}}{L_{e0}^2}\right)\left(\frac{\psi_{eA} u_e v_e}{s_e^2}\right) \tag{27c}$$

$$\left|\frac{\tau_{xzb}}{\sigma_{y0}}\right| + \left|\frac{\sigma_{zzb}}{2\sigma_{y0}}\right| \leqslant \sqrt{2}\left(\frac{A_{e0}}{L_{e0}^2}\right)\left(\frac{\psi_{eA} u_e v_e}{s_e^2}\right) \tag{27d}$$

Combining Eq. (10a) to (27a) and (27b) as well as Eq. (10b) to (27c) and (27d) then, the plastic yielding collapse surfaces of the regular octet-truss lattice material can be formulated as:

$$\left|\frac{\sigma_{xx}}{\sigma_{y0}}\right| + \left|\frac{\sigma_{zz}}{\sigma_{y0}}\right| \leqslant \frac{1}{3}\bar{\rho}_L \tag{28a}$$

$$\left|\frac{\tau_{xz}}{\sigma_{y0}}\right| + \left|\frac{\sigma_{zz}}{2\sigma_{y0}}\right| \leqslant \frac{1}{6}\bar{\rho}_L \tag{28b}$$

From Eq. (28), it can be deduced that for the regular octet-truss lattice material the ratios of the plastic collapse stresses to the relative density are independent of the cell elements geometry.

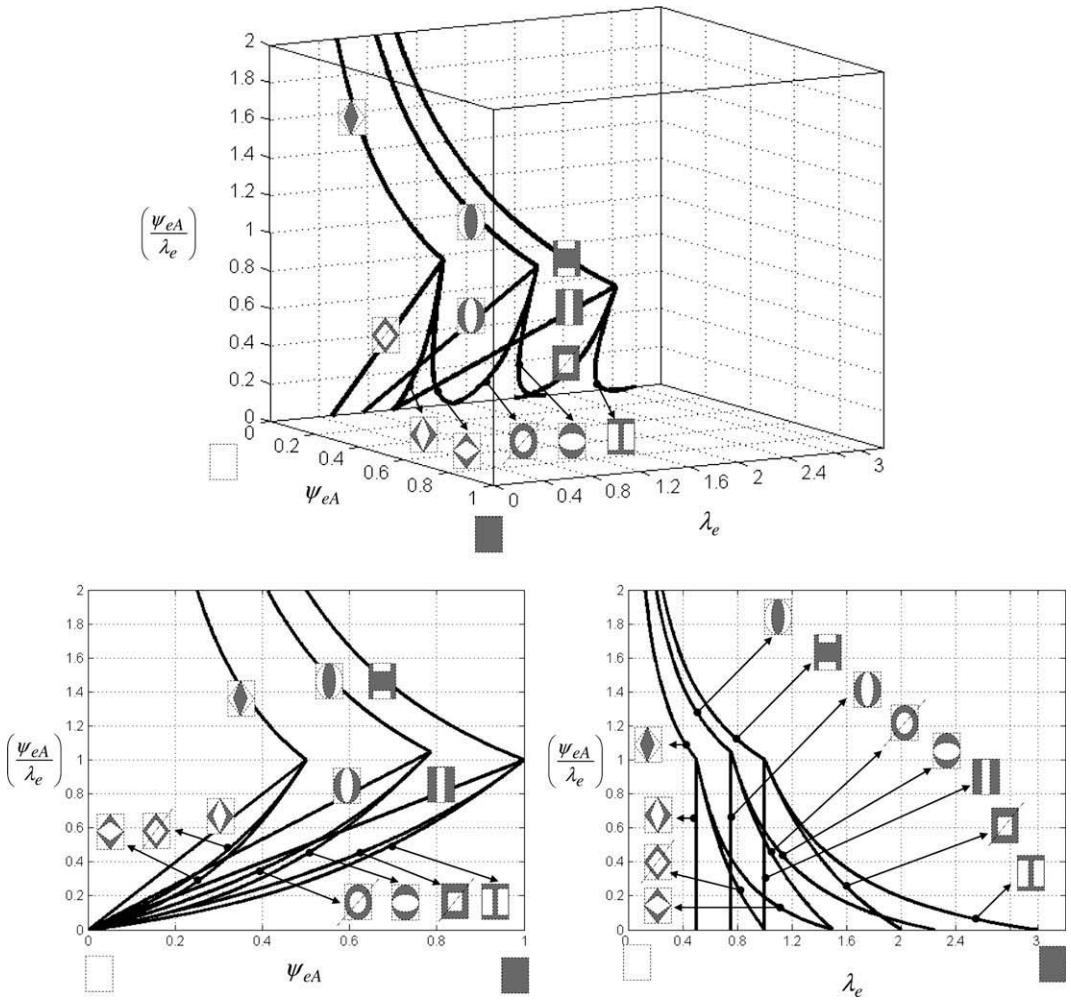

Fig. 4. Variation of the lattice material relative density with respect to cross-section efficiency and to area shape transformer.

4.4.2. Buckling collapse surfaces

Assume that the regular octet-truss cell is loaded by two forces in the x and z principal directions, as shown in Fig. 1, then, the critical buckling collapse surfaces in the x–z-plane can be formulated as:

$$\left|\frac{\sigma^{cr}_{xxa}}{\sigma_{y0}}\right| + \left|\frac{\sigma^{cr}_{zza}}{\sigma_{y0}}\right| \leqslant \left(\frac{\sqrt{2}\pi}{54}\right)\left(\frac{E_0}{\sigma_{y0}}\right)\bar{\rho}_L^2 \tag{29a}$$

$$\left|\frac{\tau^{cr}_{xza}}{\sigma_{y0}}\right| + \left|\frac{\sigma^{cr}_{zza}}{2\sigma_{y0}}\right| \leqslant \left(\frac{\pi}{54\sqrt{2}}\right)\left(\frac{E_0}{\sigma_{y0}}\right)\bar{\rho}_L^2 \tag{29b}$$

$$\left|\frac{\sigma^{cr}_{xxb}}{\sigma_{y0}}\right| + \left|\frac{\sigma^{cr}_{zzb}}{\sigma_{y0}}\right| \leqslant \left(\frac{\pi^2}{18\sqrt{2}}\right)\left(\frac{r^2_{eg0}}{A_{e0}}\right)\left(\frac{E_0}{\sigma_{y0}}\right)\left(\frac{\lambda_e}{\psi_{eA}}\right)\left(\frac{\nu_e}{u_e}\right)\bar{\rho}_L^2 \tag{29c}$$

$$\left|\frac{\tau^{cr}_{xzb}}{\sigma_{y0}}\right| + \left|\frac{\sigma^{cr}_{zzb}}{2\sigma_{y0}}\right| \leqslant \left(\frac{\pi^2}{36\sqrt{2}}\right)\left(\frac{r^2_{eg0}}{A_{e0}}\right)\left(\frac{E_0}{\sigma_{y0}}\right)\left(\frac{\lambda_e}{\psi_{eA}}\right)\left(\frac{\nu_e}{u_e}\right)\bar{\rho}_L^2 \tag{29d}$$

By normalizing Eqs. (28a), (29a) and (29c) with respect to the relative density of the lattice material, we can express the collapse surfaces as:

Yield (for a circular and a generic cross-section)

$$\left|\frac{\sigma_{xx}}{\sigma_{y0}}\right| \Big/ \bar{\rho}_L + \left|\frac{\sigma_{zz}}{\sigma_{y0}}\right| \Big/ \bar{\rho}_L \leqslant \frac{1}{3} \tag{30a}$$

Buckling (for a circular cross-section)

$$\left|\frac{\sigma^{cr}_{xxa}}{\sigma_{y0}}\right| \Big/ \bar{\rho}_L + \left|\frac{\sigma^{cr}_{zza}}{\sigma_{y0}}\right| \Big/ \bar{\rho}_L \leqslant \left(\frac{\sqrt{2}\pi}{54}\right)\left(\frac{E_0}{\sigma_{y0}}\right)\bar{\rho}_L \tag{30b}$$

Buckling (for a generic cross-section)

$$\left|\frac{\sigma^{cr}_{xxb}}{\sigma_{y0}}\right| \Big/ \bar{\rho}_L + \left|\frac{\sigma^{cr}_{zzb}}{\sigma_{y0}}\right| \Big/ \bar{\rho}_L \leqslant \left(\frac{\pi^2}{18\sqrt{2}}\right)\left(\frac{r^2_{eg0}}{A_{e0}}\right)\left(\frac{E_0}{\sigma_{y0}}\right)\left(\frac{\lambda_e}{\psi_{eA}}\right)\left(\frac{\nu_e}{u_e}\right)\bar{\rho}_L \tag{30c}$$

The relative direct stresses normalized with respect to the material relative density are plotted in Fig. 5.

For octet-truss lattice material with cell elements of circular solid cross-sections, the parameter "p", which represents the relative strength to the relative density ratio, is expressed as:

$$p_a = \left(\frac{\sqrt{2}\pi}{54}\right)\left(\frac{E_0}{\sigma_{y0}}\right)\bar{\rho}_L \tag{31a}$$

For a generic cell element cross-sections, the parameter p is expressed as:

$$p_b = \left(\frac{\pi^2}{18\sqrt{2}}\right)\left(\frac{r^2_{eg0}}{A_{e0}}\right)\left(\frac{E_0}{\sigma_{y0}}\right)\left(\frac{\lambda_e}{\psi_{eA}}\right)\left(\frac{\nu_e}{u_e}\right)\bar{\rho}_L \tag{31b}$$

The impact of shaping cell element cross-sections on the strength to mass ratio of the lattice material is shown in the following examples.

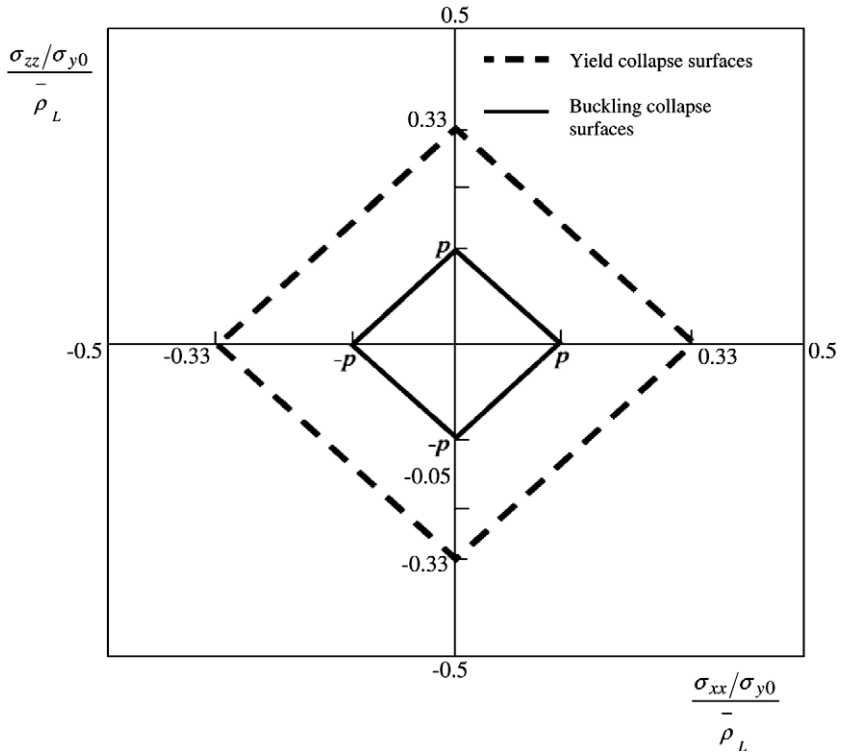

Fig. 5. Elastic and plastic collapse surfaces of the octet-truss lattice material evaluated for the relative direct stresses and normalized with respect to the material relative density.

5. Examples

5.1. Example 1

Consider an octet-truss lattice material with relative density of $\bar{\rho}_L = 0.0174$ that is manufactured of steel AISI L2 (tempered at 205 °C) which has compressive yield strength of 1835 MPa, a Young's modulus of 210 GPa and a density of 7940 kg/m^3. Starting with a preliminary design, the structural performance of the lattice material is compared in two scenarios:

(a) The lattice material has cell elements of circular solid cross-sections of radius $a_e = 0.2557$ mm and length $L_e = 10$ mm. If these values are substituted into Eq. (31a), we obtain $p_a = 0.164$.
(b) The lattice material has generic cell elements with geometrical attributes that have the values of $u_e = 2.5$, $v_e = s_e = 1$, $L_{e0} = 10$ mm, $A_{e0} = 0.4107$ mm^2, $r_{eg0} = 0.185$ mm, and $\psi_{eA} = 0.2$. Similarly, substituting these values into Eq. (31b) gives $p_b = 0.129\lambda_e$.

Assume that the generic cross-sections have efficiency $\lambda_e = 1$, then, the lattice material in both cases (a) and (b) fails by elastic buckling. However, as explained in the previous sections, an axially loaded structure that fails by buckling is far from optimum since the material fails before reaching its yielding strength, therefore, we optimize our design by increasing the buckling resistance until it coincides with the plastic yield strength. In the case of the circular solid cross-sections, this strategy results in increasing the relative density of the lattice material from 0.0174 to 0.035. On the other hand, in the case of cell element with generic cross-sections, the relative density of the material can be left constant, while the shape of the cross-section can be tuned to generate an efficiency of $\lambda_e = 2.56$. This value can be provided by a cross-section of the rectangular family with a geometry described, for example, by $c = 1$ and $d = 0.849$. As a result, shaping the cell element cross-sections of the regular octet-truss lattice material with $\lambda_e = 2.56$ increases the stress carrying capacity of the material from $(\sigma/\sigma_{y0})/\bar{\rho}_L = 0.164$ to $(\sigma/\sigma_{y0})/\bar{\rho}_L = 0.33$ and reduces the structural weight of 50%.

5.2. Example 2

In this second example, the effect of changing the efficiency of alternative cell element cross-sections on the collapses surfaces is investigated. In particular, the cross-section efficiency of the cell elements is optimized in order to increase the buckling resistance until it reaches the material yielding.

Assume a solid material with yield strain $\varepsilon_{y0} = 0.05$, and assume that the cross-section geometry of the cell elements is described by $A_{e0} = 4$ μm^2, $u_e = v_e = 1$, and has shape properties of $\psi_{eA} = 0.6$ and element length $L_e = 1$ cm. Using the derived expressions, from previous sections that characterize the lattice material properties, those properties can be computed as:

Relative density:

$$\bar{\rho}_L = \frac{\rho_L}{\rho_0} = 6\sqrt{2}\left(\frac{\psi_A A_{D0} u v}{L_e^2}\right) = 0.203 \tag{32a}$$

Plastic collapse surface:

$$\left|\frac{\sigma_{xx}}{\sigma_{y0}}\right| + \left|\frac{\sigma_{zz}}{\sigma_{y0}}\right| \leqslant 0.0676 \tag{32b}$$

Elastic buckling collapse surface:

$$\left|\frac{\sigma^{cr}_{xxb}}{\sigma_{y0}}\right| + \left|\frac{\sigma^{cr}_{zzb}}{\sigma_{y0}}\right| \leqslant 0.0445\lambda_e \tag{32c}$$

As expected, Eq. (32c) depends on the cell element cross-section efficiency, λ_e, of the lattice material. Resorting to the cross-section selection chart, shown in Fig. 6, the efficiency of alternative cross-section shapes can be determined.

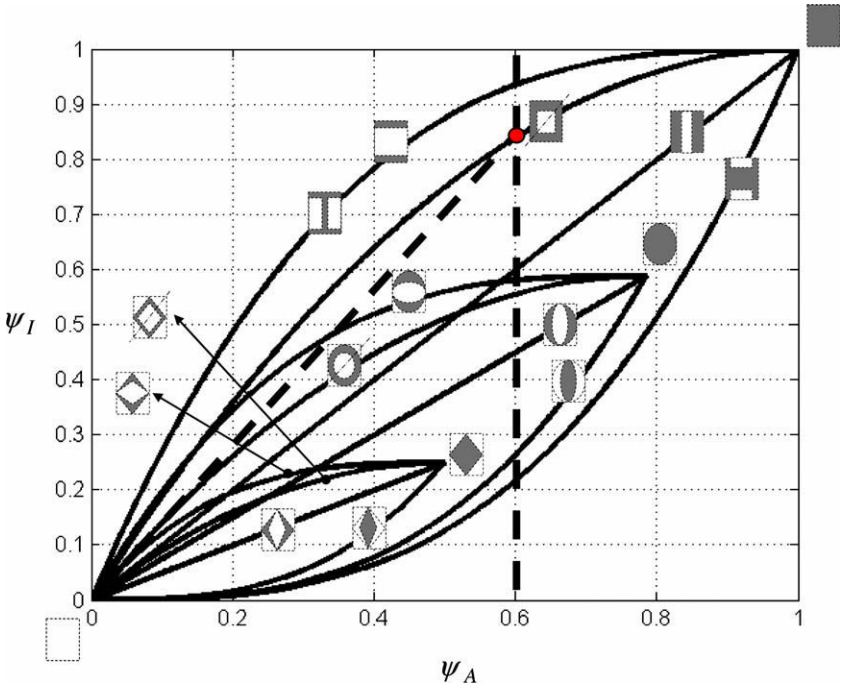

Fig. 6. Efficiencies of different cross-section shapes at specified $\psi_A = 0.6$.

In Fig. 6, we constrained the area shape transformer ($\psi_{eA} = 0.6$) which contributes to the lattice material density. The condition $\psi_{eA} = 0.6$ is illustrated by the dashed vertical line that intersects the limiting curves of the alternative cross-section shapes available. The cross-section efficiency, λ_e, is simply the slope of a segment connecting a point to the origin of the chart.

If we determine the value of the efficiency, λ_e, of the cross-section from Fig. 6 and substitute it into Eq. (32c), then, the collapse surfaces can be obtained (Fig. 7) for the cross-sections meeting the requirement $\psi_{eA} = 0.6$.

In Fig. 7, the plastic yielding collapse surfaces are superimposed to the elastic buckling collapse surfaces of the lattice material under the load case corresponding to two direct stresses in the x–z-plane. Fig. 7 shows four failure modes corresponding to Mode I $= \left(+\frac{\sigma_{xx}^{cr}}{\sigma_{y0}}, +\frac{\sigma_{zz}^{cr}}{\sigma_{y0}}\right)$, Mode II $= \left(+\frac{\sigma_{xx}^{cr}}{\sigma_{y0}}, -\frac{\sigma_{zz}^{cr}}{\sigma_{y0}}\right)$, Mode III $= \left(-\frac{\sigma_{xx}^{cr}}{\sigma_{y0}}, -\frac{\sigma_{zz}^{cr}}{\sigma_{y0}}\right)$ and Mode VI $= \left(-\frac{\sigma_{xx}^{cr}}{\sigma_{y0}}, +\frac{\sigma_{zz}^{cr}}{\sigma_{y0}}\right)$.

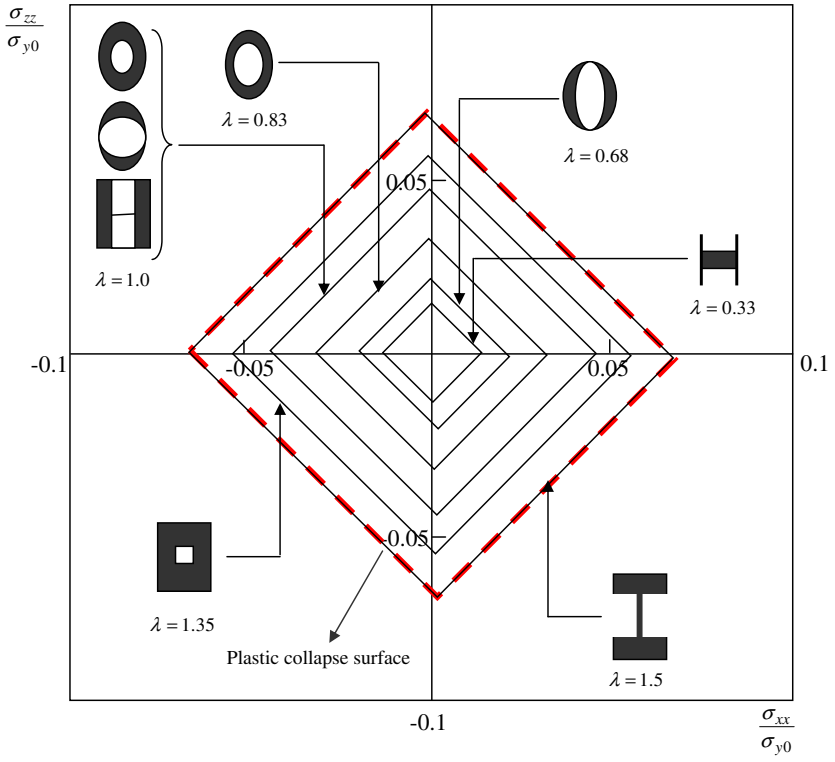

Fig. 7. Elastic and plastic collapse surfaces and the effect of cross-section efficiency on the structural performance.

The optimum lattice material is obtained when the elastic buckling resistance is increased until it is equal to the yielding failure strength (Ashby, 2005; Weaver and Ashby, 1997). In this example, such a criterion is achieved for $\lambda_e = 1.5$, which can be satisfied, for example, by a rectangular cross-section with $c = 1$ and $d = 0.48$. Although higher efficiencies can be obtained, no increase in the structural performance can be achieved, as for $\lambda_e > 1.5$ the plastic yielding will dominate the failure mode.

Whereas prescribed in this example, the cell element length will be considered as design variable in the next sections.

6. Design charts for the regular octet-truss lattice material

A design chart is developed here to help selecting the microscopic attributes of the regular octet-truss lattice material that best minimizes its relative density for a given strength requirement σ_L. The cell element length multiplier, s_e, as well as the shape of a double symmetry cross-section are considered as design variables.

For the purpose of developing such a chart, we formulate the problem in optimization terms as follows:

$$\begin{array}{ll} \text{Minimize} & \bar{\rho}_L \\ \text{With respect to} & s_e \text{ and } \psi_{eA} \\ \text{Subject to} & \sigma_e^{cr} = \sigma_{yL} = \sigma_L \\ & \text{and } u_e/v_e \geqslant 1 \end{array} \tag{33}$$

The equality constraint (33) is imposed to use the material strength to its maximum extent.

Before plotting the chart, we rearrange in three steps the expressions of the objective function $\bar{\rho}_L$ and the constraint $\sigma_e^{cr} = \sigma_{yL}$. The goal is to make them functions solely of the geometric variables of the cell element, which include the cell element length multiplier, s_e, and the cross-section efficiency λ_e.

Step (1) s_e is reformulated by substituting Eqs. (18a) and (21b) into Eq. (33), which results in the expression:

$$s_e = (\pi)\left(\frac{r_{eg0}}{L_{e0}}\right)(v_e)\sqrt{\left(\frac{E_0}{\sigma_{y0}}\right)\lambda_e} \tag{34}$$

In Eq. (34), the cell element length multiplier is controlled by the cell element cross-section shape through $\sqrt{\lambda_e}$. For convenience, we redefine s_e with the following parameter Ω_e as:

$$\Omega_e := \left(\left(\frac{L_{e0}}{r_{eg0}}\right)s_e\right) \Big/ \left(\pi v_e \sqrt{\frac{E_0}{\sigma_{y0}}}\right) = \sqrt{\lambda_e} \tag{35}$$

Step (2) The octet-truss lattice material yield strength σ_{yL} is expressed as a function of Ω_e and ψ_{eA}. Here, Eq. (35) is used to reformulate s_e in terms of Ω_e and to substitute the result into Eq. (18a), which is rewritten as:

$$\bar{\sigma}_{yL} = \frac{\sigma_{yL}}{\sigma_{y0}} = \left(\frac{\sqrt{2}}{\pi^2}\right)\left(\frac{A_{e0}}{r_{eg0}^2}\right)\left(\frac{\sigma_{y0}}{E_0}\right)\left(\frac{\psi_{eA}}{\Omega_e^2}\right)\left(\frac{u_e}{v_e}\right) \tag{36}$$

By rearranging Eq. (36), the contribution of the cell element geometry to the strength of the lattice material can be isolated, and σ_{yL} can be redefined as:

$$\sigma_{yL}^* := \frac{\sigma_{yL}}{\left(\frac{\sqrt{2}}{\pi^2}\right)\left(\frac{A_{e0}}{r_{eg0}^2}\right)\left(\frac{\sigma_{y0}}{E_0}\right)\left(\frac{u_e}{v_e}\right)} = \left(\frac{\psi_{eA}}{\Omega_e^2}\right) \tag{37}$$

Step (3) Finally, the objective function, $\bar{\rho}_L$, is expressed in terms of the design variables. From Eq. (35), s_e is expressed in terms of Ω_e and the resulting expression is substituted into Eq. (10b), which is then written as:

$$\bar{\rho}_L = C_e \frac{\psi_{eA}}{\Omega_e^2} \tag{38}$$

where $C_e = \left(\frac{6\sqrt{2}}{\pi^2}\right)\left(\frac{A_{e0}}{r_{eg0}^2}\right)\left(\frac{1}{v_e^2}\right)\left(\frac{\sigma_{y0}}{E_0}\right)$. As noted previously, Eq. (38), similarly to Eq. (36), is dependent on $\frac{\psi_{eA}}{\Omega_e^2}$ through the coefficient C_e.

The previous relations are now plotted into the design chart shown in Fig. 8. The lightest lattice materials that minimize $\frac{\psi_{eA}}{\Omega_e^2}$ in Eq. (38) are the solutions displayed at the left-top corner. The black lines, which guide the choice of Ω_e, represent the cell element lengths, Eq. (35), of different cross-section shapes. Iso-stress contours σ_{yL}^*, Eq. (37), are also superimposed to help the designer to select the best cell element cross-section shape and its length for a given σ_L requirement.

Since σ_L is specified by the problem, Eq. (37) is used to determine σ_{yL}^*, after having scaled the element cross-section with a value of u_e/v_e that meets the strength requirement. Although a specific ratio of u_e/v_e can be generated by an infinite combinations of values of u_e and v_e, in practice the maximum dimension of the cubic envelope of the microscopic octet-truss lattice cell must be limited by the minimum dimensions of the structure at the macroscopic scale.

7. Multiscale design of an axially loaded macroscopic member

The chart presented in the previous section helps design the lattice material at the microscale. In this section, the design of a real macroscopic pin-jointed strut manufactured of octet-truss lattice material is examined. The structure is subjected to a compressive force F with octet-truss lattice material properties ρ_L (density), E_L (Young's modulus) and σ_{yL} (yield strength). The lattice material is manufactured of a solid material that has density, ρ_0, Young's modulus, E_0, and yield strength, σ_{y0}. As mentioned in Section 3, the macroscale parameters are specified by the subscript G.

Section 7.1 examines the design chart for a macroscale strut; Section 7.2. presents the multiscale design of the strut, which involves the simultaneous use of both the micro- and macroscale design charts.

7.1. Design chart for macroscopic strut

Similar to the previous section, we pose the design problem of the strut under compressive force F as follows:

$$\begin{array}{ll} \text{Minimize} & m \\ \text{With respect to} & s_G \text{ and } \psi_{GA} \\ \text{Subject to} & s_f \sigma = \sigma_{yL} \leqslant \sigma_G^{cr} \\ & u_G \geqslant v_G \end{array}$$

where m is the mass of the macroscopic structure, s_G is the strut length, σ_{yL} is the yield point of the strut, s_f is a design safety factor and σ is the axial stress generated by the external force F. To develop the macroscopic structure design chart, we rearranged the above expression in three steps.

Step (1) Similar to the microscopic cell element length multiplier, s_e, the macroscopic strut length multiplier, s_G, is formulated as:

$$s_G \leqslant (\pi)\left(\frac{r_{Gg0}}{L_{G0}}\right)(v_G)\sqrt{\left(\frac{2}{3}\right)\frac{E_0}{\sigma_{y0}}\lambda_G} \tag{39}$$

Now, Eq. (39) is rearranged to isolate the macroscopic cross-section geometrical parameters where a new expression of s_G is redefined as:

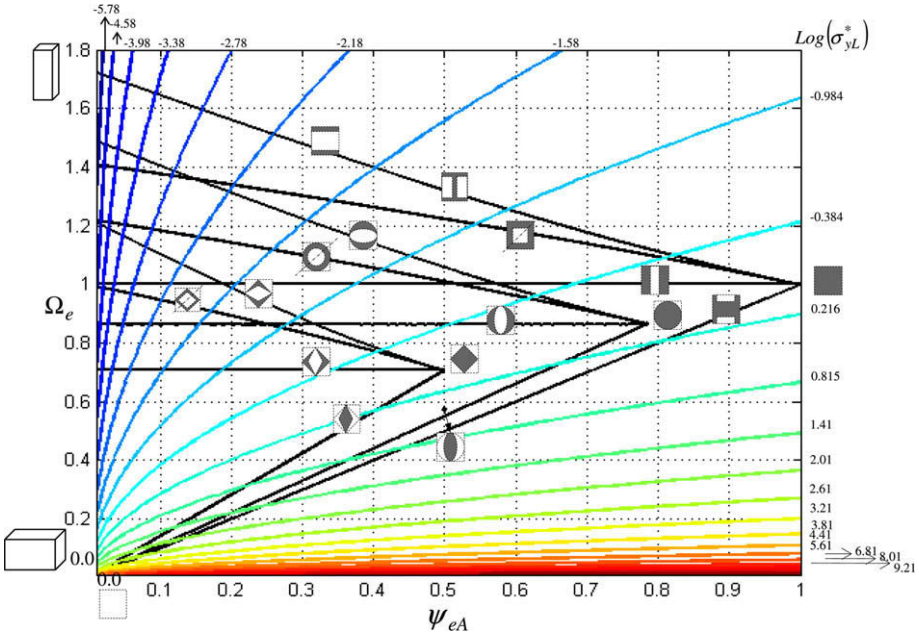

Fig. 8. Design chart of the microscopic architecture of 3D lattice materials.

$$\Omega_G := \frac{s_G}{(\pi)\left(\frac{r_{Cg0}}{L_{G0}}\right)(v_G)\sqrt{\left(\frac{2}{3}\right)\left[\frac{E_0}{\sigma_{y0}}\right]}} \leqslant \sqrt{\lambda_G} \tag{40}$$

Step (2) To avoid the yielding of the macroscopic strut under the compressive loading, F, the yield constraint $s_f\sigma = \sigma_{yL}$, is written as a function of the external force, F, such that:

$$s_f\frac{F}{A_G} = \frac{s_f F}{A_{G0}\psi_G u_G v_G} = \sigma_{yL} \tag{41}$$

Isolating v_G in Eq. (40), and substituting its expression into Eq. (41) results in:

$$\sigma_{yL} := \frac{s_f F\pi\sqrt{\left(\frac{2}{3}\right)\frac{E_0}{\sigma_{y0}}}}{\left(\frac{L_{G0}}{r_{Cg0}}\right)A_{G0}s_G u_G}\frac{\Omega_G}{\psi_{GA}} \tag{42}$$

In Eq. (42), the cross-section shape contribution is isolated and the strut yielding point is redefined as:

$$\sigma^*_G = \left(\frac{\left(\frac{L_{G0}}{r_{Cg0}}\right)A_{G0}s_G}{s_f F\pi\sqrt{\left(\frac{2}{3}\right)\frac{E_0}{\sigma_{y0}}}}\right)(u_G)(\sigma_{yL}) = \frac{\Omega_G}{\psi_{GA}} \tag{43}$$

Step (3) The objective function, m, is expressed in terms of the design variables as:

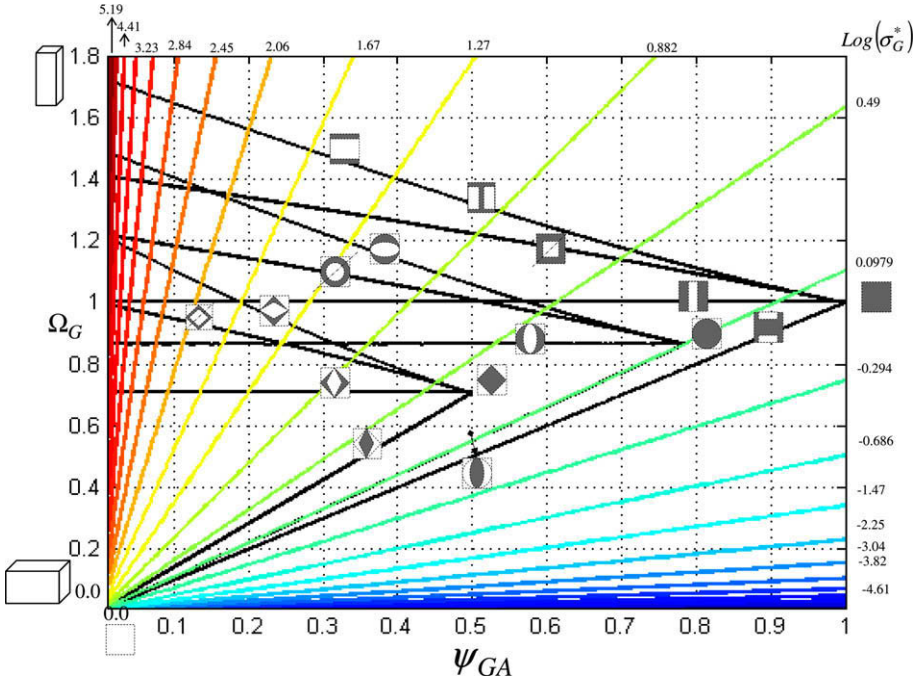

Fig. 9. Design chart of mechanical members loaded in axial compression.

$$m = C_G \bar{\rho}_L \Omega_G \psi_{GA} \tag{44}$$

where $C_G = \left(\pi\sqrt{\frac{2}{3}}\right)(A_{G0} r_{Gg0})\left(\rho_0\sqrt{\frac{E_0}{\sigma_{y0}}}\right)(u_G v_G^2)$.

Fig. 9 visualizes the macroscopic design chart that can be used to select the best geometrical attributes of a strut in axial compression for a given macroscopic loading. In Fig. 9, the black lines are the plots of Eq. (40), obtained for different cross-section shapes. They represent the correspondent strut length multiplier, s_G, which is determined from Ω_G through Eq. (40), after the cross-section height is scaled with the value of v_G that meets the load requirement. In addition, Eq. (43) is plotted in Fig. 9 to represent iso-stress lines that intersect the curves Ω_G. From this chart, the designer can select the best element length and cross-section shape of the macroscopic strut.

Next section shows how to combine Figs. 8 and 9 for a multiscale design of a lattice structural member.

7.2. Multiscale design charts

We consider a multiscale design problem which involves the optimization of a column manufactured of octet-truss lattice material at both the micro- and the macroscales. The design requirements are set at the structure as well material level. At the column level, the length, L_G, the external load, F, and the design safety factor, s_f, are prescribed; at the material scale the requirements include the solid material properties of the yield strength, σ_{y0}, the Young's modulus, E_0, and the density, ρ_0. For the reference element, the baseline of the geometric parameters are r_{eg0}, A_{e0} and L_{e0} at the microscale and L_{G0}, r_{Gg0} and A_{G0} at the macroscale.

In this problem, the objective of fully exploiting the material strength at each length scale requires the design of a column in which the three failure modes, namely, the local buckling σ_e^{cr} (buckling of the microscopic cell elements), global buckling σ_G^{cr} (buckling of the macroscopic structure) and the plastic yielding failure of the strut σ_{yL}, occur simultaneously, i.e. $\sigma_e^{cr} = \sigma_{yL} = \sigma_G^{cr}$. The rationale behind is the following: if any of the three failure modes dominates the structural failure, any performance enhancement that shifts the other two failure modes to higher limits will not contribute to the global structural performance (Weaver and Ashby, 1997). Based on this criterion, we now combine the charts shown in Figs. 8 and 9 to design a column made out of regular octet-truss lattice material.

At the macroscale, we first determine the column length multiplier, $s_G = L_G/L_{G0}$, from which we calculated Ω_G through Eq. (40), after scaling the cross-section with v_G to meet the load requirement. When Ω_G is obtained, the cross-section shape of the strut can be selected in Fig. 9 for different values of the constraint σ^*_{GyL}. Substituting the selected σ^*_{GyL} into Eq. (43) allows obtain the plastic strength σ_{yL} that will be used as an input in Fig. 8 for the design of the lattice material. σ_{yL} is then used in Fig. 8 to determine σ^*_{eyL} through Eq. (37), after scaling the cell element cross-section with the appropriate u_e/v_e, as explained in Section 6. The obtained value σ^*_{eyL} corresponds to an iso-stress line, whose intersections with Ω_e define the cell element multiplier of the lattice. The criterion to use when moving along such an iso-stress line is that of minimizing the mass of the structure, i.e. minimizing the density of the lattice material. As described in Eq. (38), the lattice materials that best minimize $\frac{\psi_{eA}}{\Omega_e^2}$ are the solutions displayed at the left-top corner of Fig. 8.

8. Conclusion

Under compression, a column manufactured of regular solid material experiences two types of failure modes, namely, the global buckling and the yield failure. A lattice material column, on the other hand, may also fail for either the local buckling or yielding of its microscopic cell element. To fully exploit the strength of a strut made of lattice material, the global buckling and the yielding failures must occur simultaneously with the microscopic failure modes. To achieve this, this paper introduced a set of multiscale design charts for the selection of the geometric properties for both the cell elements and the column cross-section. The charts help to gain insight into the impact that the structural geometry at both the micro- and macroscale has on the overall resistance of the column.

References

Ashby, M.F., 2005. Materials Selection in Mechanical Design, third ed. Elsevier/Butterworth–Heinemann, Amsterdam/London.

Beer, F.P., Johnston, E.R., 1981. Mechanics of Materials. McGraw-Hill International Book Company, New York.

Deshpande, V.S. et al., 2001. Effective properties of an octet truss lattice material. Journal of the Mechanics and Physics of Solids 49, 1747–1769.

Deshpande, V.S., Fleck, N.A., 2001. Collapse of truss core sandwich beams in 3-point bending. International Journal of Solids and Structures 38, 6275–6305.

Fan, H.L. et al., 2008. Yield surfaces and micro-failure mechanism of block lattice truss materials. Journal of Material and Design 29, 2038–2043.

Guest, S.D., Hutchinson, J.W., 2003. On the determinacy of repetitive structures. Journal of the Mechanics and Physics of Solids 51, 383–391.

Kruth, J.P. et al., 2005. Benchmarking of different SLS/SLM processes as Rapid Manufacturing techniques. In: International Conference of Polymers and Moulds Innovations (PMI) Gent, Belgium, April 20–23, pp. 1–7.

Pasini, D. et al., 2003. Structural efficiency maps for beams subject to bending. Journal of Material, Design and Applications 217, 207–220.

Pasini, D. et al., 2006. A method for selecting macro-scale structures with axially loaded members. International Journal of Mechanics and Materials Design 3 (2), 185–199.

Pasini, D., 2007. Shape transformers for material and shape selection of lightweight beams. Journal of Material and Design 28 (7), 2071–2079.

Renton, J.D., 2002. Elastic Beams and Frames, second ed. Horwood Publishing Limited, Chichester.

Rochus, P. et al., 2007. New applications of rapid prototyping and rapid manufacturing (RP/RM) technologies for space instrumentation. Acta Astronautica 61, 352–359.

Wadley, Hayden N.G., 2002. Cellular metals manufacturing. Advanced Engineering Materials 10, 726–733.

Waterman, Norman A., Dickens, Philip, 1994. Rapid product development in the USA, Europe and Japan. World Class Design to Manufacture 1 (3), 27–36.

Weaver, P.M., Ashby, M.F., 1997. Material limits for shape efficiency. Progress in Materials Science 41, 61–128.